Stabilizing the Heavily-doped and Metallic Phase of MoS_2 Monolayers with Surface Functionalization

Hanyu Zhang[1]; Tamara D. Koledin[1]; Xiang Wang[2,3]; Ji Hao[1]; Sanjini U. Nanayakkara[1]; Nuwan H. Attanayake[1]; Zhaodong Li[1]; Michael V. Mirkin[2]; and Elisa M. Miller[1]*

[1]Materials, Chemistry, and Computational Science Directorate, National Renewable Energy Laboratory, Golden Co
[2]Department of Chemistry, Queens College-CUNY, Flushing, NY, 11367 USA
[3]Chemistry Program, Graduate Center of CUNY, New York, NY, 10016 USA

*corresponding author: elisa.miller@nrel.gov

Abstract

Monolayer molybdenum disulfide (MoS_2) is one of the most studied two-dimensional (2D) transition metal dichalcogenides that is being investigated for various optoelectronic properties, such as catalysis, sensors, photovoltaics, and batteries. One such property that makes this material attractive is the ease in which 2D MoS_2 can be converted between the semiconducting (2H) and metallic/semi-metallic (1T/1T') phases or be heavily n-type doped 2H phase with ion intercalation, strain, or excess negative charge. Using n-butyl lithium (BuLi) immersion treatments, we achieve 2H MoS_2 monolayers that are heavily n-type doped with shorter immersion times (10 – 120 mins) or conversion to the 1T/1T' phase with longer immersion times (6 – 24 h); however, these doped/converted monolayers are not stable and promptly revert back to the initial 2H phase upon exposure to air. To overcome this issue and maintain the modification of the monolayer MoS_2 upon air exposure, we use BuLi treatments plus surface functionalization p-$(CH_3CH_2)_2NPh$-MoS_2 (Et_2N-MoS_2)—to maintain heavily n-type doped 2H phase or the 1T/1T' phase, which is preserved for over 2 weeks when on indium tin oxide (ITO) or sapphire substrates. We also determine that the low sheet resistance and metallic-like properties correlate with the BuLi immersion times. These modified MoS_2 materials are characterized with confocal Raman/photoluminescence, absorption, X-ray photoelectron spectroscopy as well as scanning Kelvin probe microscopy, scanning electrochemical microscopy, and four-point probe sheet resistance measurements to quantify the differences in the monolayer optoelectronic properties. We will demonstrate chemical methodologies to control the modified monolayer MoS_2 that likely extend to other 2D transition metal dichalcogenides, which will greatly expand the uses for these nanomaterials.

Keywords: MoS_2 monolayers, n-doping, phase conversion, diazonium functionalization, air-stable

1. Introduction

Molybdenum disulfide (MoS_2) monolayers are a promising material for various applications, such as catalysis, quantum computing, gas sensors, batteries, and biosensors due to the tunable electronic structure, low toxicity, flexibility, and low cost.[1–7] MoS_2 is one of the most studied transition metal dichalcogenides, where the layered materials are held together via van der Waals forces and have optoelectronic properties that are determined by the layer numbers.[8] It has been shown that MoS_2 monolayers are 3 atoms thick and have a direct band gap in its thermodynamically stable, semiconducting phase (2H or also referred to as 1H for the monolayer).[9]

To make the most of MoS_2 monolayers, it is essential that the optoelectronic properties are readily controlled and manipulated for any application. As-grown monolayer MoS_2 by chemical vapor deposition (CVD) without intentionally doping is typically an n-type semiconducting material; however, this can be tuned by changing growth conditions and growing on different substrates.[10–14] One such desired property is phase engineering MoS_2 monolayers between its 2H phase and the unstable metallic/semi-metallic (1T/1T') phase using excess negative charge, strain, and defects.[5,15–21] The 1T MoS_2 monolayer is metallic with an octahedral geometry, whereas the 1T' phase has a small bandgap (theoretically predicted to be 10s to 100s meV, depending on the level of theory) [22–24] and a distorted octahedral geometry but still exhibits metallic-like properties.[20,25,26] Monolayers of 1T/1T' MoS_2 can be useful because of the low sheet resistance for energy storage as well as an active basal plane for catalysis.[5,27] Based on previous studies, the 1T phase is not stable and readily relaxes to the 1T' phase; therefore, all the metallic-like MoS_2 monolayers will be referred to as 1T'.[22]. In addition to these extremes, MoS_2 can also exist in the 2H phase but be heavily n-type doped, where the Fermi level lies near/at the conduction band minimum and the bandgap is reduced.[28–32]

Monolayers can be beneficial over nanosheets (many layers thick) because they are essentially all surface, thinner, and can be grown in large areas. However, there are limited studies explicitly demonstrating good stability of n-type doped 2H phase or 1T' phase MoS_2 monolayers in air. [33,34] A 2021 report highlighted electron doping MoS_2 monolayers using KOH/benzo-18-crown-6 to stabilize the doped MoS_2 for over 1 month in air.[34] On the contrary, it has been well documented that MoS_2 nanosheets can be (partially) converted to the 1T' phase and survive for a limited time in air.[35–37] To extend the shelf life and use of these 1T' MoS_2 nanosheets, one strategy is to functionalize the metallic MoS_2 with surface groups to "lock-in" the metallic properties.[38] In cases where uniform, monolayer coverage with a large lateral area is required or beneficial,[31,39] one must be able to confidently control and manipulate the optoelectronic properties of monolayers—similar to the nanosheets. However, monolayers are more sensitive to their surroundings than nanosheets.[25] Therefore, the focus of this study is to experimentally demonstrate the use of chemical functionalization to control and stabilize the 1T' phase or heavily n-type doped 2H phase of MoS_2 monolayers.

Here, we manipulate MoS_2 monolayers from 2H to heavily n-type doped 2H to 1T' using n-butyl lithium (BuLi) immersion treatments, where n-butyl lithium has been used to phase convert MoS_2 monolayers previously and is based on bulk MoS_2 exfoliation.[38,40,41] A shorter BuLi immersion time (10 – 120 mins) heavily n-type dopes MoS_2 while a longer BuLi immersion time (>2 hr) converts the MoS_2 from 2H to 1T' phase when the monolayers are supported on indium tin oxide (ITO) or sapphire substrates. We show with various spectroscopic, microscopic, and electronic transport techniques that the heavily n-type doped 2H/1T' phase is not stable in air and reverts back to the initial 2H phase before the appropriate measurements can be performed. To stabilize the n-type doped 2H and 1T' phase, we functionalize the surface using a diazonium salt to form $(CH_3CH_2)_2NPh\text{-}MoS_2$ ($Et_2N\text{-}MoS_2$). Our various characterization techniques confirm that the heavily n-type doped 2H and 1T' phase is maintained in air and that the degree of sheet resistance can be tuned by the BuLi immersion time. The addition of Et_2N functional groups to MoS_2, allows the heavily n-type doped 2H and 1T' phase of MoS_2 monolayers to be used in air, which could be more readily incorporated into various nanodevices.

2. Materials and Methods

Single Crystal Monolayer Growth. Si with 300-nm thermal oxide layer (University Wafers) was cut and annealed in a 550 °C oven for 10 min. The substrate was spin-coated with 300 µL of precursor—made up of supernatant saturated MoO_3 (Sigma Aldrich, 99.97% purity, powder) and 0.02-M NaOH solution (Fisher Scientific, $\geq$ 97.0% purity pellets) with ultrapure water (18.2 MΩ)—at 1600 rpm for 50 sec. Single crystal monolayer MoS_2 was grown via chemical vapor deposition (CVD) in a three-chamber furnace under atmospheric pressure (625 Torr) with a 50 sccm argon gas flow. The method is modified from a previous report.[42] The furnace temperatures were 530 °C, 800 °C, and 800 °C for zone 1, 2, and 3, respectively, with a ramp-up rate at 35 °C/min. The precursor loaded silicon substrate was placed in the end of the third zone. Solid sulfur precursor pellets were placed upstream in an alumina boat, and the closed system was purged with argon three times. The sulfur was heated to 180 °C for 8 min with heat tape when zone 3 of the furnace reached 700 °C. The furnace and heat tape were turned off, and the sample was left to cool with argon flow until the furnace temperature was 150 °C. This process resulted in single crystal, isolated triangles of MoS_2 monolayers with sizes up to 30 microns. The single-crystal monolayer MoS_2 samples were characterized by photoluminescence spectroscopy (PL), X-ray photoelectron spectroscopy (XPS), scanning Kelvin probe microscopy (SKPM) and scanning electrochemical microscopy (SECM).

Transfer of Single Crystal Monolayer MoS_2 to Substrates. A polystyrene solution (PS, average molecular weight ~192,000, Sigma-Aldrich) was spin-coated on the MoS_2 grown Si sample at 3000 rpm for 60 s. The PS coated sample was put in a 150 °C oven for 5 min, and then the edges were scratched with a razor blade. The PS/MoS_2 sample on Si/SiO_2 was slowly immersed in 80 °C 2 M NaOH solution until the PS/MoS_2 film fully peels off from the Si/SiO_2. The floating film was then fishing out with glass slide, and transferred into ultrapure water, and lastly extracted with the new substrate, i.e., ITO. The sample was soaked in toluene for 20 min, rinsed with ultrapure water, and annealed in an N_2 environment for 30 min at 200 °C.

Continuous-film Monolayer Growth. Continuous monolayer MoS_2 was adapted from a previous report.[43] The large-area MoS_2 was grown in a 1-Torr CVD environment with an argon flow of 80 sccm and argon with 4% O_2 at 6 sccm. A precursor, 2 mg MoO_3, was placed in zone 2 of the furnace. Approximately 2 g of sulfur was placed prior to zone 1. A <0001> sapphire wafer (University Wafer) was used and bath-sonicated in acetone, isopropanol, and ultrapure water for 10 min each before being placed at the end of zone 3. The closed system was purged with argon three times and the furnace was heated to 530 °C, 930 °C, and 930 °C for zone 1, 2 and 3, respectively. The temperatures were maintained for 35 min before turning off the furnace. The system was left to cool with argon flow until the furnace reached 150 °C. The continuous monolayer MoS_2 samples on as-grown on sapphire were used for UV-Vis absorption and 4-point probe measurements.

Doping/Converting 2H MoS_2 and Surface-functionalization: The 2H MoS_2 monolayers were immersed into fresh 2.5 M n-butyl lithium (BuLi, Sigma Aldrich) for various times in a N_2 glovebox. To achieve repeatable results, the BuLi had to be fresh without any visible precipitates. BuLi solution residue can be removed by hexane (Sigma Aldrich). To add functional groups to the MoS_2, the BuLi treated monolayers were immediately put into 10 mg/mL 4-p-diazo-N,N-Diethylaniline fluoroborate (MP Biomedicals) aqueous solution for 30 min. The functionalized monolayer samples were immersed into 50-mL isopropyl alcohol (J.T. Baker) and rinsed two times with 100-mL ultrapure water sequentially to remove the excess or weakly bound aniline groups. The resulting sample films were then characterized.

X-ray Photoelectron Spectroscopy (XPS). Single crystal MoS_2 monolayer films transferred onto ITO were transferred to the XPS setup via an air-free transfer vessel. XPS data were obtained on a Physical Electronics 5600 system using Al Kα radiation. The XPS setup was calibrated with Au metal, which was cleaned via Ar-ion sputtering. The raw atomic concentration has a 5% error due to surface inhomogeneities, surface roughness, literature sensitivity values for peak integration, *etc*. The air-free films were measured under ultra-high vacuum (10^{-9} Torr), then the samples were removed from vacuum and set on the lab bench for 20 mins before being measured again under ultra-high vacuum.

UV-Vis Absorption Spectroscopy. The absorption was collected by Cary 5000 series UV/Vis spectrophotometer (Agilent Technology). The inert environment was achieved by the airtight sample holder with transparent windows. The samples used for these measurements were as-grown continuous MoS_2 monolayers on sapphire.

Confocal Raman Spectroscopy and Photoluminescence (PL). Raman and PL spectroscopy was performed on a Renishaw inVia (Gloucestershire, UK) by using a 532-nm laser and 100× magnification or 50× long working distance objective lenses. The scattering light from the sample was directed by a grating with 1800 lines/mm for Raman or 600 lines/mm for PL prior to the CCD detector. The Raman/PL mapping is achieved by a motorized stage with 0.3-µm step size. The typical exposure time is 2 s with 5 accumulations to reduce the instrumentational noise. The samples used here were single crystal MoS_2 monolayer films transferred onto ITO. For the air-free measurements, we used an airtight sample holder with transparent windows.

Scanning Kelvin Probe Microscopy (SKPM). SKPM measurements were performed in air using single pass mode on a Park AFM equipped with an XE-70 controller and an external lock-in amplifier (SR830, Stanford Research Systems). Measurements were made with an electrical AC bias applied on the tip, using lock-in detection and feedback at 18 kHz for the surface potential signal. Conductive Pt/Ir-coated AFM cantilevers (Multi-75EG, Budget Sensors) were used for SKPM imaging. Topography was measured at the first resonance frequency (~70 kHz) and potential was collected with a 1.00 V AC bias at 18 kHz, well-separated from the topography frequency.

Scanning Electrochemical Microscopy (SECM). SECM experiments were carried out using the home-built setup as described previously,[44] including the three-electrode setup with a 0.25-mm diameter Ag wire coated with AgCl serving as a reference electrode, a 1-mm Pt wire counter electrode, and an unbiased substrate. Pt nanoelectrodes with the tip radius, $a \approx 120$ nm (calculated from the diffusion-limited current of 1 mM ferrocenemethanol), were fabricated by pulling and heat sealing 25 µm diameter Pt wires into borosilicate glass capillaries under vacuum with a P-2000 laser pipet puller. The fabricated nanoelectrodes were polished on a 50-nm alumina pad (Precision Surfaces International) under video microscopic control. Appropriate protection was used to avoid electrostatic damage to the nanotips.

The tip was brought within about 30 µm vertical distance from the substrate using a manual micromanipulator and an optical microscope. Then, the tip was moved toward the substrate using the z-piezo stage over ~25 µm distance with a relatively high approach velocity (e.g., 0.5 µm/s). An approach curve was obtained with a slower velocity (e.g., 40 nm/s). All experiments were carried out at room temperature inside a Faraday cage.

Feedback mode of the SECM operation was used to image the monolayers. In a feedback mode experiment, the SECM probe was brought within a short distance from the MoS_2 monolayer immobilized on a flat, conductive ITO surface. The electrolyte contained a redox mediator ferrocenemethanol (Fc) and the tip potential (E_T) was such that the mediator oxidation occurred at a rate governed by diffusion. With the separation distance between the tip and substrate (d) sufficiently small (i.e., comparable to a), the oxidized form of the mediator (Fc^+) produced at the tip surface was reduced at the substrate, and the tip current increased with decreasing d (positive feedback; the tip current near the surface was higher than its value in the bulk solution; $i_T > i_{T,\infty}$). If the regeneration rate of the mediator at the substrate was slow, i_T decreased with decreasing d because of the hindered diffusion of Fc (negative feedback; $i_T < i_{T,\infty}$). An image was obtained by scanning the tip laterally (in the x-y plane) over the sample surface.

Four-point Probe Measurements. The typical Four-point probe measurement was performed by using Signatone four-point resistivity measurement system with a custom-developed LabVIEW program. All measurements were conducted inside the N_2-filled glovebox in the dark. For each sample on the sapphire substrate, current vs. voltage curves of at least 5 different positions were measured and recorded.

3. Results and Discussion

In order to stabilize the heavily n-type doped 2H and 1T' phase of MoS_2 monolayers in air, we develop a modified protocol based on a previous report with BuLi treatments and surface functionalization (Figure 1).[38] For these studies, we use CVD grown monolayers of 2H MoS_2 (Figure 1a), which can be transferred from the growth substrate Si/SiO_X onto other substrates if needed for characterization; the monolayer growth and transfer are detailed in the **Materials and Methods Section**. The transferred MoS_2 monolayers onto ITO or the continuous film MoS2 monolayers on sapphire maintain the thermodynamically stable 2H phase until we intentionally alter it with BuLi immersion treatments.

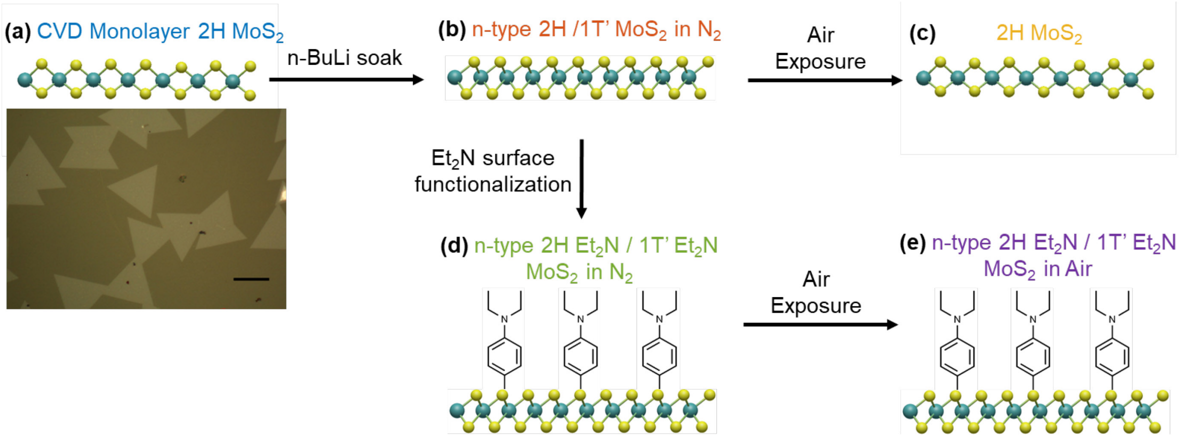

Figure 1. Schematic of the experiment design flow for doping/converting and Et_2N functionalizing MoS_2 monolayers. (a) CVD grown monolayer MoS_2 transferred onto ITO. Microscope image showing the MoS_2 monolayers with a 15 µm scale bar. (b) Heavily n-type doped 2H or 1T’ phase monolayer MoS_2 after immersing in BuLi solution under inert N_2 environment. (c) After air exposure, the heavily n-type doped 2H or 1T’ monolayer MoS_2 de-dopes/reverts back to 2H phase. (d) Heavily n-type doped 2H or 1T’ monolayer MoS_2 after surface functionalization with Et_2N diazonium solution in N_2. (e) Retained modification of monolayer MoS_2 after air exposure.

As shown in the schematic in Figure 1, we start with 2H MoS_2 (Figure 1a) and immerse the monolayer film in BuLi in a N_2 glovebox to convert the MoS_2 from 2H to heavily n-type doped 2H or 1T’ phase (Figure 1b). Once the monolayer is exposed to air, the MoS_2 de-dopes/converts back to the initial 2H (Figure 1c). To stabilize the heavily n-type doped 2H or 1T’ phase, we add Et_2N functional groups to the monolayer in the glovebox (Figure 1d), which stabilizes the materials for at least 2 weeks in air (Figure 1e). The doping/phase of the MoS_2 monolayers is measured using UV-Vis absorption spectroscopy, confocal PL spectroscopy, and XPS (Figure 4) as well as Raman spectroscopy (Figure 2 and 7). We confirm the materials are monolayer by the splitting of the A_1’ and E’ Raman features (Figure 2a), the strong PL (Figure 3b), and atomic force microscopy measurements (Figure 5). Note that our CVD growth does not produce exclusively MoS_2 monolayers; therefore, the UV-Vis absorption, XPS, and 4-point probe measurements may have some signal from multilayer growth that is within our measurement detection area.

3.1 30-min BuLi Immersion Time

Raman spectroscopy is a valuable tool for evaluating MoS_2 layer thickness, phase, and doping. For these studies, we use confocal Raman microscopy with 1-micron spatial resolution to characterize the MoS_2 monolayers following various treatments. Monolayer MoS_2 has the point group D_{3h}.[45] Therefore, A_1’ and E’ are used to identify the out-of-plane and in-plane stretching modes, respectively, instead of A_{1g} and E_{2g} that are used for multilayers. Our transferred 2H MoS_2 has a ~18.6 cm^{-1} A_1’/E’ splitting, which is in agreement with a monolayer (Figure 2a).[46] Once the monolayer is treated with BuLi for 30 mins, we measure the Raman spectrum in a N_2 environment to determine if the monolayer has been electron doped or phase converted. The A_1’ peak red shifts by ~1.7 cm^{-1}, while the E’ peak position is constant, which has been recently shown to be attributed to n-type doping of MoS_2 monolayers.[33] Furthermore, we do not observe the typical J peaks associated with the 1T/1T’ phase of MoS_2 (extended spectra shown in Figure S1).[47,48] The A_1’ red shift and lack of J peaks is a result of softened out-of-plane vibrations through weakening S-Mo bonds due to electron density occupying the antibonding states in the conduction band, yet not enough electron transfer for phase conversion to 1T/1T’ with a 30-min BuLi immersion treatment.[29,49] Note, we will expand upon this n-type doped 2H/1T’ phase differentiation more in the next section.

To closely evaluate how the 30-min BuLi immersion and functionalization affects the MoS_2 monolayer, we use Raman mapping of the same MoS_2

triangle following each treatment. For the 2H MoS_2 sample, the A_1' peak position has a small (~1 cm^{-1}) variation around 404 cm^{-1} across the entire monolayer, which provides us with a baseline (Figure 2b). Following a 30-min BuLi immersion time, the A_1' mapping (Figure 2c) reveals that the peak is evenly red shifted (~403 cm^{-1}) and that n-type doping is throughout the monolayer. The E' peak position is unaffected by the BuLi treatment and results in an A_1'/E' splitting of ~17.1 cm^{-1} (Figure 2a). Once the MoS_2 monolayer is exposed to air, the A_1' peak blue shifts to ~405 cm^{-1} (Figure 2d), which is slightly higher (~0.5 cm^{-1}) than the initial 2H MoS_2 and is probably due to the de-doped monolayer becoming slightly oxidized (see XPS results below). Likely, this de-doping is an electron-withdrawing process via an oxidizing agent in air (i.e., O_2 or H_2O molecules).[50] Therefore, when considering MoS_2 monolayers, the fact that we cannot even perform the measurements before the sample reverts to the initial 2H MoS_2 is noteworthy and would be challenging to use if heavily n-type doped 2H MoS_2 monolayers are needed in an air-exposed application.

In our previous MoS_2 nanosheets study, we were able to elongate the shelf-life of the 1T/1T' MoS_2 nanosheets with surface functionalization.[38] Therefore, taking notes from this previous study, we use surface functionalization to extend the lifetime of the modified MoS_2 monolayers in air. Specifically, we use the BuLi treated monolayers in a glove box and immerse the film into 4-p-diazo-N,N-diethylaniline fluoroborate aqueous solution. This results in bound p-$(CH_3CH_2)_2NPh$ functional groups to the n-type doped 2H MoS_2 monolayer, where the n-type 2H Et_2N-MoS_2 samples are kept under a N_2 environment for the Raman measurements. The A_1' peak red shifts by ~2.7 cm^{-1} and the E' slightly red shifts by ~0.8 cm^{-1} (Figure 2e). Therefore, the ~16.9 cm^{-1} A_1'/E' splitting along with the greater red shift of A_1' leads us to conclude that Et_2N functionalized MoS_2 in air is also heavily n-type doped and that the surface functionalization results in an overall ~1 cm^{-1} red shift. Once the monolayer is exposed to air, the mapping data reveals the n-type 2H Et_2N-MoS_2 in air is homogeneously n-type doped throughout the monolayer (Figure 2f), with only a small blue shift of A_1' compared to the sample in N_2. The Raman spectroscopy allow us to determine the 30-min BuLi immersion time results in heavily n-type doping of the MoS_2 monolayers that is stabilized in air when functionalized with Et_2N. Other characterization techniques are used to measure the 30-min BuLi treated MoS_2 monolayers.

The monolayer A and B exciton features are well-known indicators for the direct bandgap, semiconducting 2H phase of MoS_2, which reflects the spin-orbit splitting of the valence band maximum at the K point in the Brillouin zone. In Figure 3a, the absorption spectrum of continuous MoS_2 (2H-MoS_2) monolayer shows clear A and B exciton transitions at ~610 and ~660 nm, which matches the previous reports for monolayer MoS_2.[51] After immersing the monolayers in BuLi for 30 min (Figure 3a), both the A and B exciton features disappear as long as the treated monolayers remain in an inert environment. The loss of the exciton features is expected due to electron

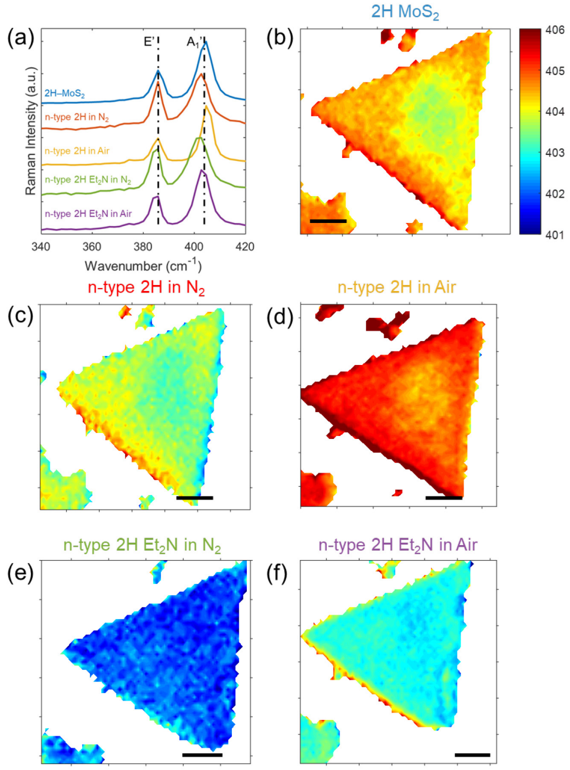

Figure 2. Confocal Raman spectroscopy of MoS_2 with 30-min BuLi immersion time. (a) Raman spectra of the A_1' and E' vibrational modes of the MoS_2 monolayer under various conditions. (b-f) A' peak position mapping regarding the same MoS_2 monolayer under various conditions, namely (b) 2H MoS_2 on ITO, (c) 30-min BuLi immersed MoS_2 in N_2, (d) 30-min BuLi immersed MoS_2 in air, (e) 30-min BuLi immersion followed by Et_2N surface-functionalization of MoS_2 in N_2, and (f) 30-min BuLi immersion followed by Et_2N surface-

transfer from the strong reducing agent (BuLi) to MoS_2.[52–54] The n-type doped 2H MoS_2 monolayer sample is unstable when exposed to ambient air. The A and B excitons start to grow-in as the MoS_2 de-dopes back to the initial doping level during the UV-Vis absorption measurement when performed under ambient conditions (Figure 3a). These absorption measurements take ~10 min, which is enough time to restore the A and B exciton features back to the intensity of the initial 2H phase of MoS_2.

Upon surface functionalization and air exposure, the A and B excitons of MoS_2 are still suppressed (Figure 3a), which indicates the surface functionalization maintains the n-type doping. The A and B exciton features remain relatively suppressed for several weeks as the A and B excitons slowly grow in under ambient conditions (Figure S2). Our results demonstrate that the surface functionalization provides a unique way to maintain the heavily n-type doping of MoS_2 monolayers.

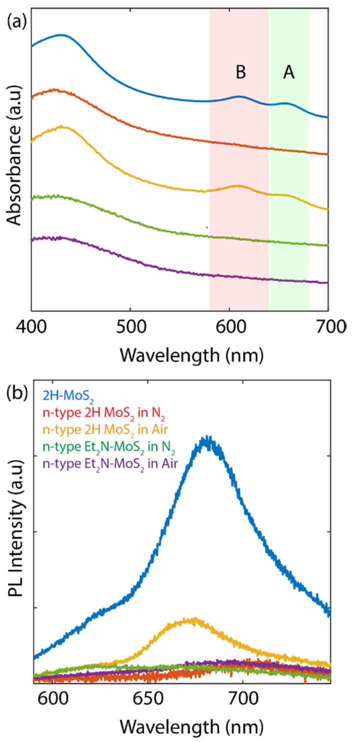

Figure 3. Spectroscopy of MoS_2 with 30-min BuLi immersion time. (a) UV-Vis absorption spectra of continuous MoS_2 monolayer under various conditions. (b) PL of single crystal MoS_2 monolayers transferred onto ITO. The legend in panel (b) applies to both figure panels.

To further confirm the stabilization of the n-type doped 2H phase of MoS_2 monolayers, we use confocal PL, where we measure the PL from one monolayer triangle (Figure 3b). The initial 2H MoS_2 (transferred onto ITO) demonstrates the highest PL intensity at ~680 nm and corresponds to emission from the A exciton.[34] The A exciton emission is quenched when the monolayers are treated with BuLi for 30 mins, which is similar to a previous n-type doping experiments.[34,56] However, the PL grows in when the n-type doped 2H phase MoS_2 monolayers are exposed to air. The PL is blue shifted by 5 nm (~675 nm) and is likely due to a slightly oxidized surface (see XPS results). By adding Et_2N functional groups to the BuLi treated monolayers, the PL remains minimized in N_2 and ambient air conditions (Figure 3b). These results strongly agree with the Raman and UV-Vis absorption data and demonstrate the stability of n-type doped 2H phase MoS_2 monolayers in air when adding the Et_2N functional groups.

Similar conclusions can also be drawn from the XPS results. We measure two samples one where the transferred MoS_2 monolayers are treated with BuLi for 30 mins and one where the monolayers are treated with BuLi for 30 mins followed by aqueous 4-p-diazo-N,N-diethylaniline fluoroborate in a glovebox. These samples are subsequently transferred air-free to the XPS setup and measured with XPS (Figure 4b and 4d). Once XPS measurements on the air-free samples are complete, the same samples are exposed to air for 20 mins on the lab benchtop before re-measuring with XPS (Figure 4c and 4e). We also have a reference 2H MoS_2 sample for comparison (Figure 4a). For these measurements, we have a detection area of ~1 mm^2; therefore, the XPS data are mostly MoS_2 monolayers but can also contain few layer triangles.

The structural phase and/or doping of MoS_2 can be determined by the Mo^{+4} peak positions, where Mo *3d* transitions have two peaks due to spin-orbit coupling that are split by 3.13 eV. The XPS data show two distinct Mo^{+4} environments for all treated MoS_2 monolayers: an environment consistent with intrinsic 2H (i-2H: 229/232 eV) and a lower binding energy peak, which we attribute to heavy n-type doping (n-2H: 228/231 eV—will be explained in more detail below). By fitting the Mo^{+4} peaks, we quantify the amount of n-2H vs i-2H MoS_2 character, where the fits are shown in Figure 4. As reference, we only observe the peak of i-2H environment from untreated 2H

MoS_2. For the 30-min BuLi treated MoS_2 in N_2, the XPS data yields ~50% n- 2H to 50% i-2H MoS_2 character. After exposing the sample to air for 20 mins, our measurements show that the i-2H character increases: ~40% n-type 2H to 60% i-2H MoS_2 character. However, with Et_2N surface functionalization of n-type 2H MoS_2, the XPS Mo *3d* spectra are similar between the air-free and air-exposed monolayers, ~65% n-2H to 35% i-2H MoS_2.

Overall, the n-type 2H Et_2N-MoS_2 sample has more n-2H character than the unfunctionalized, 30 min-BuLi treated MoS_2 monolayer (Figure 4). The different ratios between the air-free samples emphasize the instability of the unfunctionalized, n-type doped 2H MoS_2 monolayer, where it starts to revert to its initial 2H state during our air-free transfer, which can be a few hours before we perform the XPS measurement. These results agree with the UV-Vis absorption and PL data—emphasizing that the Et_2N surface functionalization stabilizes the n-type doped 2H phase.

If the 30-min BuLi treatment simply n-type doped the MoS_2 monolayers, we would expect the 2H MoS_2 peaks to shift to higher binding energy, which is typical for n-type doping.[57,58] However, this is not what we measure. What we observe are peak positions that are lower in electron binding energy and similar to 1T/1T' MoS_2 peak positions (228/231 eV).[37,59] Therefore, the XPS results suggest that the electron doping collapses the bandgap. According to theoretical reports on degenerately n-type doping 2H MoS_2 monolayers, the bandgap does not collapse but decreases by a few hundred meV.[60,61] Therefore, a likely explanation is electron doping strains the 2H MoS_2 lattice, which together with electron doping collapses the 2H bandgap and results in the lower electron binding energy XPS features. This conclusion is in alignment with previous MoS_2 studies evaluating the correlation between strain and electron doping.[12,53,62] Additional high-resolution microscopy studies (e.g., transmission electron microscopy or scanning tunneling microscopy) are needed to confirm this hypothesis and are beyond the scope of this work.

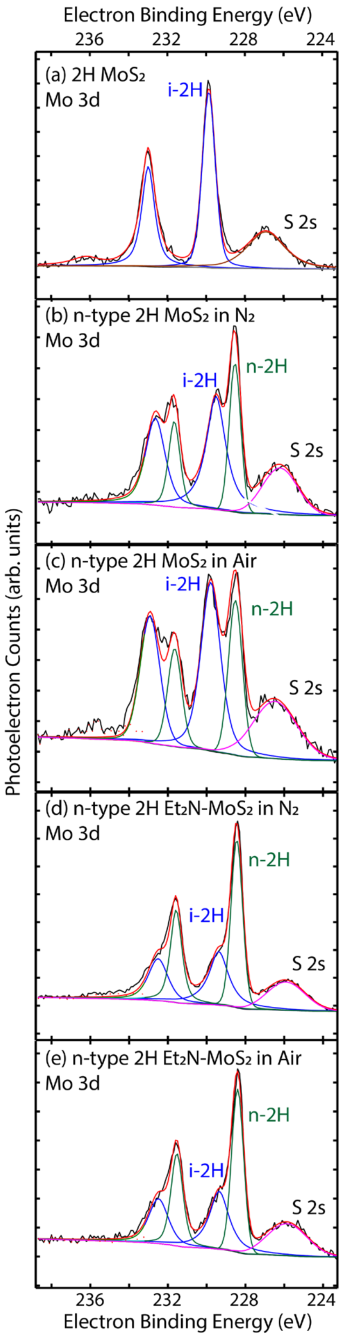

Figure 4. XPS of the Mo *3d* region of MoS_2. (a) XPS of untreated 2H MoS_2 is shown for reference. Also, XPS of 30-min BuLi treated MoS_2 in (b) N_2 then (c) exposed to air for 20 mins is shown. Similarly, the 30-min BuLi treated plus Et_2N functionalized MoS_2 in (d) N_2 and then (e) exposed to air for 20 mins is shown. The lowest energy peak is due to S *2s*, which overlaps with the Mo *3d* spectra. The Mo 3d spectra is fit to two different types of Mo^{+4} environments: i-2H and n-2H.

In addition to Mo *3d* spectra, we also acquired S *2p* (Figure S3a) and N *1s* spectra (Figure S3b) of the MoS_2 monolayers. The S *2p* has spin-orbit peaks that are separated by 1.18 eV. Like Mo *3d*, the S *2p* peak positions are dependent on the MoS_2 character, where lower energy transitions (~161.5 eV) have n-2H character and the higher binding energy transitions (~162.5 eV) have i-2H character. As expected, the S *2p* peak positions trend similarly to the Mo *3d* peak positions. The S *2p* spectra shows a slight oxidation of the n-type doped 2H MoS_2 monolayers compared to the n-type doped 2H Et_2N-MoS_2, resulting in higher binding energy features (~168 eV). For the unfunctionalized n-type doped 2H MoS_2 sample, the increased oxidation and 2H component stresses the instability and reactivity of this MoS_2 compared to the functionalized monolayer. We also evaluated the N 1s spectra to confirm the Et_2N functional group. For the n-type 2H Et_2N-MoS_2 monolayer spectrum, we assign the N *1s* peak at ~400 eV to the Et_2N functional group based on previous aniline assignments.[38,63]

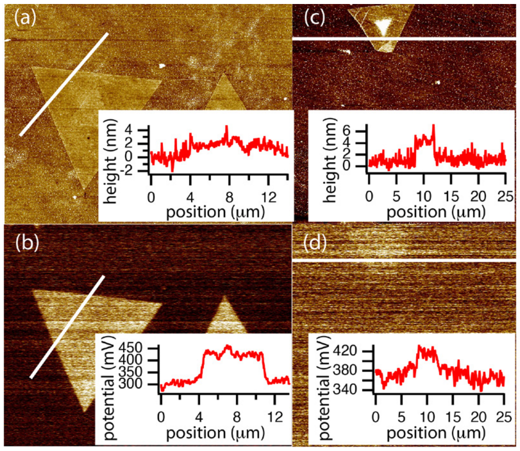

Figure 5. Comparing surface potential images of 2H- and n-type 2H Et_2N-MoS_2 on ITO. (a, c) AFM topography and (b, d) SKPM mappings of the (a, b) 2H MoS_2 on ITO and (c, d) n-type 2H Et_2N-MoS_2 on ITO in air. Note, (a) and (c) are not the identical monolayers.

The Et_2N functionalization stabilizes the change produced by the BuLi, which is similar to what we and others observed with MoS_2 nanosheets, giving a longer "shelf life".[37,38] We argue that when the surface group (Et_2N) binds to the surface, it does so by removing negative charge from the monolayers. The combination of the bound functional group and less negative charge on the monolayer "locks-in" the n-type doping or metallic phase and prevents ambient air (H_2O, O_2, CO_2) from interacting with the surface via adsorption/reaction/oxidation. Overall, the functionalization group de-energizes and prevents any rapid oxidation in air.

To further corroborate the uniform doping across the exposed top surface of these layers, we used SKPM, an AFM based technique to map the local surface potential variations and elucidate any changes to the electronic character of the 2H MoS_2 monolayers compared to the n-type 2H Et_2N MoS_2 monolayers. In addition to acquiring local surface potential information from SKPM, we are also able to measure the apparent height of the measured triangles (Figure 5a and 5c). The 2H MoS_2 height is ~1 nm and strongly suggests a monolayer. Note our AFM measurements are affected by the ITO surface roughness and transfer process. However, our PL/Raman measurements corroborate the existence of monolayer MoS_2 of the transferred samples. As expected, the apparent height of the n-type 2H Et_2N-MoS_2 monolayer is greater due to the BuLi and surface functionalization treatment.

Scanning Kelvin probe microscopy measures surface potential via detection of electrostatic forces between a conducting probe tip and the surface resulting in images that show the contact potential differences.[64] Thus, this technique can be used to elucidate qualitative, spatially resolved changes in surface potential resulting from surface functionalization. Furthermore, SKPM has a lateral resolution of ~50 nm and thus any variations greater than 50 nm in doping can be resolved. Surface potential images of 2H MoS_2 and n-type 2H Et_2N-MoS_2 are shown in Figure 5, where images are not of the same monolayer. The 2H MoS_2 has a surface potential difference from the ITO substrate (~+150 mV, Figure 5b). This is different from the n-type 2H Et_2N-MoS_2 monolayer that has close (~<+40 mV) to the same potential as the ITO substrate (Figure 5d). We use this data to qualitatively conclude that the monolayers have been uniformly modified by Et_2N surface functionalization (additional SKPM data of 2H and n-type 2H Et_2N MoS_2 samples are demonstrated in Figure S4). These SKPM results highlight how the 30-min BuLi and Et_2N surface functionalization treatment change the local workfunction uniformly across the monolayers, which could be beneficial for heterostructure energetic alignment in different applications.

To further characterize the flake surface, we use SECM to examine the local chemical reactivity

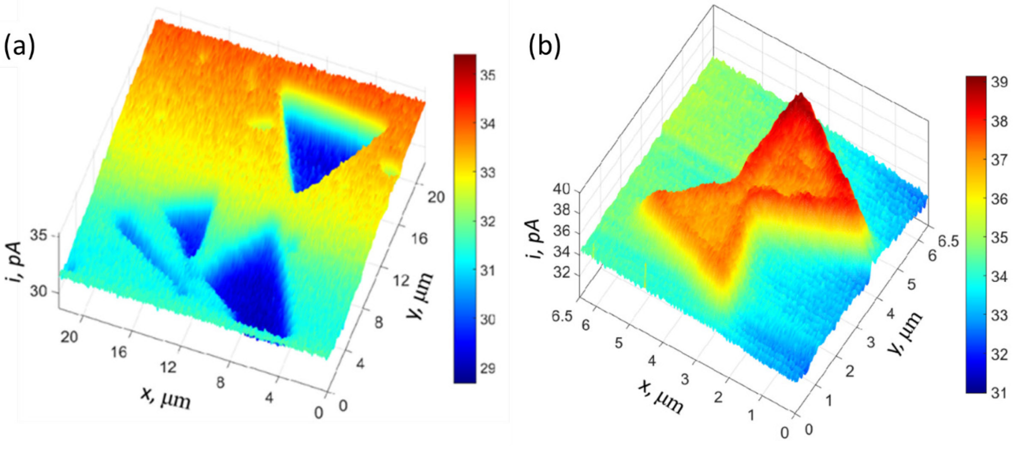

Figure 6. Comparing local electrochemical activity of 2H- and Et_2N-MoS_2 transferred onto ITO. Feedback mode SECM images of (a) 2H MoS_2 and (b) Et_2N-MoS_2 on ITO. The electrolyte for SECM is 1 mM Fc and 0.1 M KCl. E_T = 0.4 V vs. Ag/AgCl. *d* (separation distance between the tip and substrate) ≈ 40 nm and *a* (tip radius) ≈ 120 nm. The substrate was unbiased.

differences. The single crystal 2H-MoS_2 and n-type 2H Et_2N-MoS_2 samples are prepared on ITO at NREL and shipped to CUNY-Queens for SECM measurements under ambient conditions. Figures 6a and 6b show the electrochemical activity of 2H-MoS_2 and n-type 2H Et_2N-MoS_2 monolayers, respectively, imaged in the feedback mode. The sample is unbiased, and the tip biased at E_T = +400 mV (vs. Ag/AgCl) is positioned over the underlying ITO surface (d ≈ 40 nm), where the oxidation of Fc is diffusion controlled. The tip current is lower over 2H MoS_2 (29 – 30 pA) than that over the ITO surface (>31 pA) (Figure 6a) because the regeneration of the Fc mediator at the insulating 2H MoS_2 is slower than that at the ITO surface. However, the tip current (>36 pA) over the n-type 2H Et_2N-MoS_2 monolayer (Figure 6b) is higher than that over the ITO background. These measurements inform us that the n-type 2H Et_2N-MoS_2 preserves its high conductivity after the sample is shipped across the country to another lab under ambient conditions (over 2 weeks from prep to measurement). These results agree with our previous publications showing that n-type 2H Et_2N-MoS_2 is stable under electrochemical conditions and have the potential to be better suited for catalytic reactions.[38]

3.2 BuLi Immersion Time Study

As we indicated earlier, the BuLi immersion times impact the degree of doping and phase conversion. In Figure 7 and S5, we explore this further with various BuLi immersion times using Raman spectroscopy. The 30-min to 24-h BuLi immersion times are compared with and without Et_2N functionalization (Figure 7a). For the BuLi only treated MoS_2 monolayers at 30-min and 24-h immersion times, there is a significant difference between the Raman spectra. The 24-h immersion time yields the characteristic metallic J_1 and J_2 or LA peaks at ~150 cm^{-1} and ~225 cm^{-1}, respectively.[48,65,66] In general, the 24-h BuLi spectrum is relatively congested and broadened compared to the 30-min immersion time; therefore, the J_3 peak at 320 cm^{-1} could be present but not large enough to identify. The shoulders at ~290 cm^{-1} and ~350 cm^{-1} are also characteristic of the 1T/1T' phase and have been previously assigned to 1T/1T' MoS_2 phase.[48] In addition, we observe a red shift, decrease in peak intensity, and broadening of the in-plane E' peak (~385 cm^{-1}), which has been observed previously for 1T/1T' phases.[55,67] The significant and reproducible spectral differences between the 30-min and 24-h BuLi immersion times lead us to conclude that the longer immersion time fully converts the 2H MoS_2 to 1T' phase, whereas the shorter immersion time is an intermediate point that is heavily n-type doped 2H.

To stabilize the 1T' phase conversion from 2H, we add Et_2N surface functionalization groups. Figure 7a compares the 1T' Et_2N-MoS_2 to the unfunctionalized, 1T' MoS_2 at 24-h BuLi immersion times, where the 1T' Et_2N-MoS_2 (24 h) spectrum changes slightly but still has most of the characteristic 1T/1T' features, e.g. J_2 at 225 cm^{-1}, 350 cm^{-1}, and broadened red-shifted E'. Therefore, we conclude that the 1T' Et_2N functionalized MoS_2 with a 24-h BuLi immersion time

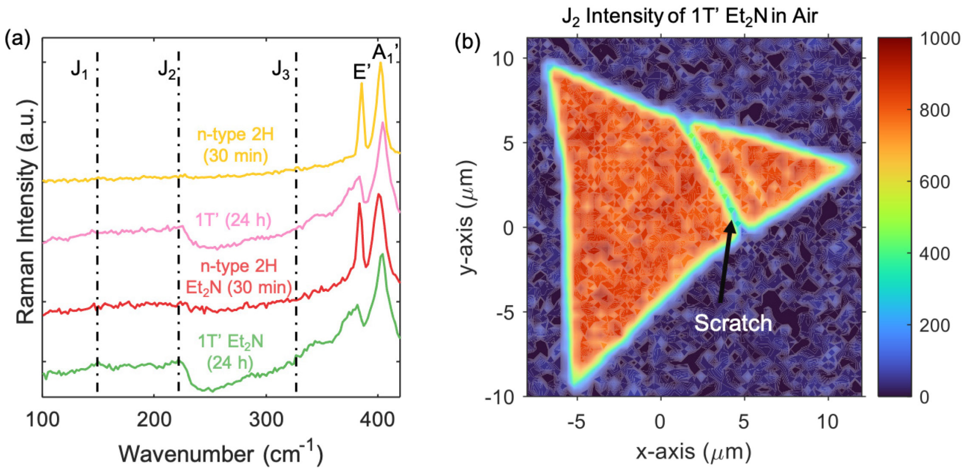

Figure 7. Raman Spectroscopy of MoS_2 monolayers following different BuLi immersion times (a) Raman spectra of MoS_2 monolayers immersed for 30 min or 24 h in BuLi with and without Et_2N surface functionalization. Measurements for the samples with Et_2N (red for 30 min BuLi soaking and green for 24 h) are conducted in air, while BuLi only treated samples (yellow and pink lines) are carried out under a N_2 environment (b) Raman mapping of the J_2 mode (~225 cm^{-1}) intensity extracted from 1T' Et_2N MoS_2 measured in air.

remains in the 1T' phase. The J_2 peak intensity is mapped across the 1T' Et_2N-MoS_2 (24 h) monolayer to show that the phase conversion is across the monolayer (Figure 7b, Figure S6 for the intensity at 380 cm^{-1} and 405 cm^{-1}). Additional Raman measurements where the BuLi immersion time is varied, shows that the n-type doping occurs with less than 10-mins BuLi immersion time and the phase conversion happens between 2-h and 6-h immersion times (Figure S5). The Raman measurements are critical in differentiating between MoS_2 monolayers being heavily n-type doped or converted to the 1T' phase, whereas UV-Vis absorption, PL, and XPS did not show differences between the BuLi immersion times. Note that when the MoS_2 monolayers are on the Si/SiO_x substrate, the surface protection of 1T' MoS_2 from Et_2N functionalization are not as effective as on ITO or sapphire substrates. (Figure S7) Understanding this difference in substrate, will be a focus of upcoming studies.

Finally, the standard four-point probe measurements are performed on the treated MoS_2 monolayers to determine the variation of sheet resistance and stability of these BuLi treated monolayers when exposed to air. Here, we use the continuous growth method for the MoS_2 monolayers on sapphire, and all four-point probe measurements are performed in a N_2 glovebox. For each panel in Figure 8, two monolayer samples are used, where the same sample is measured three times: the as grown 2H MoS_2, following treatments(s) in N_2, and then following air exposure. Figure 8a shows the variation of sheet resistance in MoS_2 monolayers with a 30-min BuLi immersion time with and without Et_2N surface functionalization. After 30-min BuLi treatment, the n-type doped 2H MoS_2 monolayers have a lower sheet resistance compared to the as-grown 2H MoS_2 for both unfunctionalized and functionalized monolayers.[68,69] When the BuLi only MoS_2 monolayers are exposed to air for 10 mins, the sheet resistance increases closer to the initial 2H state; however, the n-type 2H Et_2N-MoS_2 monolayers only have a small change when exposed to air for 10 mins. This result agrees with our previous findings that the

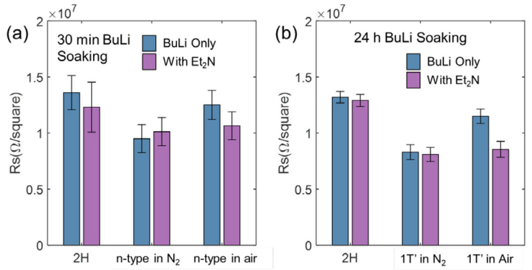

Figure 8. Four-point probe sheet resistant measurements of continuous film MoS_2 monolayers on sapphire (a) 30-min and (b) 24-h BuLi immersion times with (purple) and without Et_2N (blue) surface functionalization in N_2 and air exposure.

Et_2N surface functionalization stabilizes the n-type doping of MoS_2 in air.

We also evaluate the MoS_2 monolayers after being immersed in BuLi for 24 h with and without Et_2N functionalization (Figure 8b). In these set of measurements, we find very similar trends; however, there is a lower sheet resistance for the 24-h BuLi treatments compared to the 30-min BuLi treatments for both the unfunctionalized and functionalized monolayers in N_2. The lower sheet resistance in N_2 is due to the longer BuLi immersion time that completely converts 2H MoS_2 to 1T' MoS_2. After exposing both monolayers to air for 24 h, the sheet resistance of the BuLi only MoS_2 monolayer increases closer to the initial 2H MoS_2 sheet resistance; in contrast, the 1T' Et_2N-MoS_2 monolayer has only a small increase in sheet resistance. This air exposure highlights how the Et_2N functionalization stabilizes the 1T' MoS_2 monolayers for 24 h in air. Overall, electrical conductance measurements along with our confocal Raman results demonstrate that the immersion time of 2H MoS_2 monolayers in BuLi heavily n-type dope MoS_2 at shorter times and phase convert the MoS_2 to 1T' at longer times. Moreover, the Et_2N surface functionalization stabilizes these heavily n-type doped 2H or 1T' MoS_2 monolayers in air for extended periods of time, which will benefit the application of MoS_2 monolayers in advanced electronic devices and energy harvesting.

4. Conclusions

We report on the stabilization of heavily n-type doped 2H and 1T' MoS_2 monolayers with surface functionalization. We find that the BuLi immersion time controls the amount of electron transfer to MoS_2 monolayers on ITO or sapphire substrates, which changes the MoS_2 monolayer electronic structure. Specifically, a 10-min to 120-min BuLi immersion time will heavily n-type dope the 2H MoS_2, whereas phase conversion to 1T' occurs between 2- and 6-h BuLi immersion times. These heavily n-type doped 2H and 1T' MoS_2 monolayers are not stable when exposed to air but slightly oxidize and revert back to the initial 2H state. However, by adding Et_2N surface functionalization groups to the MoS_2 surface, we stabilize the modified MoS_2 in air. Our microscopic characterization results show that the entire MoS_2 monolayer is homogeneously n-type doped or 1T' phase converted and stabilized. Chemical control of the electronic structure of MoS_2 monolayers will be important as these monolayers are used in various applications, such as catalysis, batteries, resistors, and sensors. We speculate that this methodology for chemical control can be extended to other 2D transition metal dichalcogenides, opening a broad array of surface functionalization and strategies for use of 2D materials in novel devices and applications.

5. Acknowledgements

HZ, SUN, NA, ZL, and EMM acknowledge funding provided by U.S Department of Energy, Office of Science, Office of Basic Energy Sciences, Division of Chemical Sciences, Geosciences and Biosciences, Solar Photochemistry for the overall project direction, material growth and treatments, and all other measurements. The support of the SECM work by the National Science Foundation (CHE-1900463; MVM) is gratefully acknowledged. JH acknowledges support for the 4-point measurements from the Center for Hybrid Organic Inorganic Semiconductors for Energy (CHOISE) an Energy Frontier Research Center funded by the Office of Basic Energy Sciences, Office of Science. TK's internship is supported by the U.S. Department of Energy, Office of Science, Office of Workforce Development for Teachers and Scientists (WDTS) under the Science Undergraduate Laboratory Internship (SULI) program at NREL. The NREL authors would like to thank the Alliance for Sustainable Energy, LLC, the manager and operator of the National Renewable Energy Laboratory for the U.S. Department of Energy under Contract No. DE-AC36-08GO28308. The views expressed in the article do not necessarily represent the views of the Department of Energy or the U.S. Government. The U.S. Government retains and the publisher, by accepting the article for publication, acknowledges that the U.S. Government retains a nonexclusive, paid-up, irrevocable, worldwide license to publish or reproduce the published form of this work, or allow others to do so, for U.S. Government purposes.

6. References

[1] Yadav V, Roy S, Singh P, Khan Z and Jaiswal A 2019 2D MoS2-Based Nanomaterials for Therapeutic, Bioimaging, and Biosensing Applications *Small* **15** 1803706

[2] Venkata Subbaiah Y P, Saji K J and Tiwari A 2016 Atomically Thin MoS2: A Versatile Nongraphene 2D Material *Advanced Functional Materials* **26** 2046–69

[3] Sulas-Kern D B, Miller E M and Blackburn J L 2020 Photoinduced charge transfer in transition metal dichalcogenide heterojunctions – towards next generation energy technologies *Energy Environ. Sci.* **13** 2684–740

[4] Jiang L, Lin B, Li X, Song X, Xia H, Li L and Zeng H 2016 Monolayer MoS2–Graphene Hybrid Aerogels with Controllable Porosity for Lithium-Ion Batteries with High Reversible Capacity *ACS Appl. Mater. Interfaces* **8** 2680–7

[5] Zhang J, Wu J, Guo H, Chen W, Yuan J, Martinez U, Gupta G, Mohite A, Ajayan P M and Lou J 2017 Unveiling Active Sites for the Hydrogen Evolution Reaction on Monolayer MoS2 *Advanced Materials* **29** 1701955

[6] Luo Y K, Xu J, Zhu T, Wu G, McCormick E J, Zhan W, Neupane M R and Kawakami R K 2017 Opto-Valleytronic Spin Injection in Monolayer MoS2/Few-Layer Graphene Hybrid Spin Valves *Nano Lett.* **17** 3877–83

[7] Perkins F K, Friedman A L, Cobas E, Campbell P M, Jernigan G G and Jonker B T 2013 Chemical Vapor Sensing with Monolayer MoS2 *Nano Lett.* **13** 668–73

[8] Mak K F, Lee C, Hone J, Shan J and Heinz T F 2010 Atomically Thin MoS2: A New Direct-Gap Semiconductor *Phys. Rev. Lett.* **105** 136805

[9] Chhowalla M, Shin H S, Eda G, Li L-J, Loh K P and Zhang H 2013 The chemistry of two-dimensional layered transition metal dichalcogenide nanosheets *Nature Chemistry* **5** 263–75

[10] Sercombe D, Schwarz S, Pozo-Zamudio O D, Liu F, Robinson B J, Chekhovich E A, Tartakovskii I I, Kolosov O and Tartakovskii A I 2013 Optical investigation of the natural electron doping in thin MoS2 films deposited on dielectric substrates *Sci Rep* **3** 3489

[11] Komsa H-P and Krasheninnikov A V 2015 Native defects in bulk and monolayer ${\mathrm{MoS}}_{2}$ from first principles *Phys. Rev. B* **91** 125304

[12] Chae W H, Cain J D, Hanson E D, Murthy A A and Dravid V P 2017 Substrate-induced strain and charge doping in CVD-grown monolayer MoS2 *Appl. Phys. Lett.* **111** 143106

[13] Li M, Yao J, Wu X, Zhang S, Xing B, Niu X, Yan X, Yu Y, Liu Y and Wang Y 2020 P-type Doping in Large-Area Monolayer MoS2 by Chemical Vapor Deposition *ACS Appl. Mater. Interfaces* **12** 6276–82

[14] Xu W, Li S, Zhou S, Lee J K, Wang S, Sarwat S G, Wang X, Bhaskaran H, Pasta M and Warner J H 2018 Large Dendritic Monolayer MoS2 Grown by Atmospheric Pressure Chemical Vapor Deposition for Electrocatalysis *ACS Appl. Mater. Interfaces* **10** 4630–9

[15] Zhu J, Wang Z, Yu H, Li N, Zhang J, Meng J, Liao M, Zhao J, Lu X, Du L, Yang R, Shi D, Jiang Y and Zhang G 2017 Argon Plasma Induced Phase Transition in Monolayer MoS2 *J. Am. Chem. Soc.* **139** 10216–9

[16] Ye G, Gong Y, Lin J, Li B, He Y, Pantelides S T, Zhou W, Vajtai R and Ajayan P M 2016 Defects Engineered Monolayer MoS2 for Improved Hydrogen Evolution Reaction *Nano Lett.* **16** 1097–103

[17] Lin C-P, Chen P-C, Huang J-H, Lin C-T, Wang D, Lin W-T, Cheng C-C, Su C-J, Lan Y-W and Hou T-H 2019 Local Modulation of Electrical Transport in 2D Layered Materials Induced by Electron Beam Irradiation *ACS Appl. Electron. Mater.* **1** 684–91

[18] Lloyd D, Liu X, Christopher J W, Cantley L, Wadehra A, Kim B L, Goldberg B B, Swan A K and Bunch J S 2016 Band Gap Engineering with Ultralarge Biaxial Strains in Suspended Monolayer MoS2 *Nano Lett.* **16** 5836–41

[19] Conley H J, Wang B, Ziegler J I, Haglund R F, Pantelides S T and Bolotin K I 2013 Bandgap Engineering of Strained Monolayer and Bilayer MoS2 *Nano Lett.* **13** 3626–30

[20] Wang Z, Liu X, Zhu J, You S, Bian K, Zhang G, Feng J and Jiang Y 2019 Local engineering of topological phase in monolayer MoS2 *Science Bulletin* **64** 1750–6

[21] Peng J, Liu Y, Luo X, Wu J, Lin Y, Guo Y, Zhao J, Wu X, Wu C and Xie Y 2019 High Phase Purity of Large-Sized 1T’-MoS2 Monolayers with 2D Superconductivity *Advanced Materials* **31** 1900568

[22] Qian X, Liu J, Fu L and Li J 2014 Quantum spin Hall effect in two-dimensional transition metal dichalcogenides *Science* **346** 1344–7

[23] Zhuang H L, Johannes M D, Singh A K and Hennig R G 2017 Doping-controlled phase transitions in single-layer ${\mathrm{MoS}}_{2}$ *Phys. Rev. B* **96** 165305

[24] Hu T, Li R and Dong J 2013 A new (2 × 1) dimerized structure of monolayer 1T-molybdenum disulfide, studied from first principles calculations *The Journal of Chemical Physics* **139** 174702

[25] Li Z, Song Y and Tang S 2020 Quantum spin Hall state in monolayer 1T′-TMDCs *Journal of Physics: Condensed Matter* **32** 333001

[26] Yin X, Wang Q, Cao L, Tang C S, Luo X, Zheng Y, Wong L M, Wang S J, Quek S Y, Zhang W, Rusydi A and Wee A T S 2017 Tunable inverted gap in monolayer quasi-metallic MoS2 induced by strong charge-lattice coupling *Nature Communications* **8** 486

[27] Tian Y, Song X, Liu J, Zhao L, Zhang P and Gao L 2019 Generation of Monolayer MoS2 with 1T Phase by Spatial-Confinement-Induced Ultrathin PPy Anchoring for High-Performance Supercapacitor *Advanced Materials Interfaces* **6** 1900162

[28] Wang Y, Slassi A, Stoeckel M-A, Bertolazzi S, Cornil J, Beljonne D and Samorì P 2019 Doping of Monolayer Transition-Metal Dichalcogenides via Physisorption of Aromatic Solvent Molecules *J. Phys. Chem. Lett.* **10** 540–7

[29] Lockhart de la Rosa C J, Phillipson R, Teyssandier J, Adisoejoso J, Balaji Y, Huyghebaert C, Radu I, Heyns M, De Feyter S and De Gendt S 2016 Molecular doping of MoS2 transistors by self-assembled oleylamine networks *Appl. Phys. Lett.* **109** 253112

[30] Zou H, Zeng Q, Peng M, Zhou W, Dai X and Ouyang F 2018 Electronic structures and optical properties of P and Cl atoms adsorbed/substitutionally doped monolayer MoS2 *Solid State Communications* **280** 6–12

[31] Fang H, Tosun M, Seol G, Chang T C, Takei K, Guo J and Javey A 2013 Degenerate n-Doping of Few-Layer Transition Metal Dichalcogenides by Potassium *Nano Lett.* **13** 1991–5

[32] Dhakal K P, Ghimire G, Chung K, Duong D L, Kim S W and Kim J 2019 Probing Multiphased Transition in Bulk MoS2 by Direct Electron Injection *ACS Nano* **13** 14437–46

[33] Li M, Yao J, Liu Y, Wu X, Yu Y, Xing B, Yan X, Guo W, Tan M, Sha J and Wang Y 2020 Air stable and reversible n-type surface functionalization of MoS2 monolayer using Arg and Lys amino acids *J. Mater. Chem. C* **8** 12181–8

[34] Ogura H, Kaneda M, Nakanishi Y, Nonoguchi Y, Pu J, Ohfuchi M, Irisawa T, Lim H E, Endo T, Yanagi K, Takenobu T and Miyata Y 2021 Air-stable and efficient electron doping of monolayer MoS2 by salt–crown ether treatment *Nanoscale* **13** 8784–9

[35] Lukowski M A, Daniel A S, Meng F, Forticaux A, Li L and Jin S 2013 Enhanced Hydrogen Evolution Catalysis from Chemically Exfoliated Metallic MoS2 Nanosheets *J. Am. Chem. Soc.* **135** 10274–7

[36] Sun D, Huang D, Wang H, Xu G-L, Zhang X, Zhang R, Tang Y, Abd EI-Hady D, Alshitari W, Saad AL-Bogami A, Amine K and Shao M 2019 1T MoS2 nanosheets with extraordinary sodium storage properties via thermal-driven ion intercalation assisted exfoliation of bulky MoS2 *Nano Energy* **61** 361–9

[37] Knirsch K C, Berner N C, Nerl H C, Cucinotta C S, Gholamvand Z, McEvoy N, Wang Z, Abramovic I, Vecera P, Halik M, Sanvito S, Duesberg G S, Nicolosi V, Hauke F, Hirsch A, Coleman J N and Backes C 2015 Basal-Plane Functionalization of Chemically Exfoliated Molybdenum Disulfide by Diazonium Salts *ACS Nano* **9** 6018–30

[38] Benson E E, Zhang H, Schuman S A, Nanayakkara S U, Bronstein N D, Ferrere S, Blackburn J L and Miller E M 2018 Balancing the Hydrogen Evolution Reaction, Surface Energetics, and Stability of Metallic MoS2 Nanosheets via Covalent Functionalization *J. Am. Chem. Soc.* **140** 441–50

[39] Radisavljevic B, Radenovic A, Brivio J, Giacometti V and Kis A 2011 Single-layer MoS2 transistors *Nat Nano* **6** 147–50

[40] Voiry D, Goswami A, Kappera R, Silva C de C C e, Kaplan D, Fujita T, Chen M, Asefa T and Chhowalla M 2015 Covalent functionalization of monolayered transition metal dichalcogenides by phase engineering *Nat Chem* **7** 45–9

[41] Dines M B 1975 Lithium intercalation via -Butyllithium of the layered transition metal dichalcogenides *Materials Research Bulletin* **10** 287–91

[42] Yun S J, Han G H, Kim H, Duong D L, Shin B G, Zhao J, Vu Q A, Lee J, Lee S M and Lee Y H 2017 Telluriding monolayer MoS2 and WS2 via alkali metal scooter *Nature Communications* **8** 2163

[43] Yu H, Liao M, Zhao W, Liu G, Zhou X J, Wei Z, Xu X, Liu K, Hu Z, Deng K, Zhou S, Shi J-A, Gu L, Shen C, Zhang T, Du L, Xie L, Zhu J, Chen W, Yang R, Shi D and Zhang G 2017 Wafer-Scale Growth and Transfer of Highly-Oriented Monolayer MoS2 Continuous Films *ACS Nano* **11** 12001–7

[44] Sun T, Zhang H, Wang X, Liu J, Xiao C, Nanayakkara S U, Blackburn J L, Mirkin M V and Miller E M 2019 Nanoscale mapping of hydrogen evolution on

metallic and semiconducting MoS2 nanosheets *Nanoscale Horiz.* **4** 619–24

[45] Zhang X, Qiao X-F, Shi W, Wu J-B, Jiang D-S and Tan P-H 2015 Phonon and Raman scattering of two-dimensional transition metal dichalcogenides from monolayer, multilayer to bulk material *Chemical Society Reviews* **44** 2757–85

[46] Li H, Zhang Q, Yap C C R, Tay B K, Edwin T H T, Olivier A and Baillargeat D 2012 From bulk to monolayer MoS 2: Evolution of Raman scattering *Advanced Functional Materials* **22** 1385–90

[47] Attanayake N H, Thenuwara A C, Patra A, Aulin Y V, Tran T M, Chakraborty H, Borguet E, Klein M L, Perdew J P and Strongin D R 2018 Effect of Intercalated Metals on the Electrocatalytic Activity of 1T-MoS2 for the Hydrogen Evolution Reaction *ACS Energy Lett.* **3** 7–13

[48] Yu Y, Nam G-H, He Q, Wu X-J, Zhang K, Yang Z, Chen J, Ma Q, Zhao M, Liu Z, Ran F-R, Wang X, Li H, Huang X, Li B, Xiong Q, Zhang Q, Liu Z, Gu L, Du Y, Huang W and Zhang H 2018 High phase-purity 1T′-MoS 2 - and 1T′-MoSe 2 -layered crystals *Nature Chemistry* **10** 638–43

[49] Kiriya D, Tosun M, Zhao P, Kang J S and Javey A 2014 Air-Stable Surface Charge Transfer Doping of MoS2 by Benzyl Viologen *J. Am. Chem. Soc.* **136** 7853–6

[50] Martincová J, Otyepka M and Lazar P 2020 Oxidation of metallic two-dimensional transition metal dichalcogenides: 1T-MoS2 and 1T-TaS2 *2D Mater.* **7** 045005

[51] Jeon J, Jang S K, Jeon S M, Yoo G, Jang Y H, Park J-H and Lee S 2015 Layer-controlled CVD growth of large-area two-dimensional MoS2 films *Nanoscale* **7** 1688–95

[52] Dhakal K P, Duong D L, Lee J, Nam H, Kim M, Kan M, Lee Y H and Kim J 2014 Confocal absorption spectral imaging of MoS2: optical transitions depending on the atomic thickness of intrinsic and chemically doped MoS2 *Nanoscale* **6** 13028–35

[53] Carroll G M, Zhang H, Dunklin J R, Miller E M, Neale N R and Lagemaat J van de 2019 Unique interfacial thermodynamics of few-layer 2D MoS2 for (photo)electrochemical catalysis *Energy Environ. Sci.* **12** 1648–56

[54] Jiao Y, Hafez A M, Cao D, Mukhopadhyay A, Ma Y and Zhu H 2018 Metallic MoS2 for High Performance Energy Storage and Energy Conversion *Small* **14** 1800640

[55] Leng K, Chen Z, Zhao X, Tang W, Tian B, Nai C T, Zhou W and Loh K P 2016 Phase Restructuring in Transition Metal Dichalcogenides for Highly Stable Energy Storage *ACS Nano* **10** 9208–15

[56] Birmingham B, Yuan J, Filez M, Fu D, Hu J, Lou J, Scully M O, Weckhuysen B M and Zhang Z 2019 Probing the Effect of Chemical Dopant Phase on Photoluminescence of Monolayer MoS2 Using in Situ Raman Microspectroscopy *J. Phys. Chem. C* **123** 15738–43

[57] Li S, Chen X, Liu F, Chen Y, Liu B, Deng W, An B, Chu F, Zhang G, Li S, Li X and Zhang Y 2019 Enhanced Performance of a CVD MoS2 Photodetector by Chemical in Situ n-Type Doping *ACS Appl. Mater. Interfaces* **11** 11636–44

[58] Kaushik N, Karmakar D, Nipane A, Karande S and Lodha S 2016 Interfacial n-Doping Using an Ultrathin TiO2 Layer for Contact Resistance Reduction in MoS2 *ACS Appl. Mater. Interfaces* **8** 256–63

[59] Chang K, Hai X, Pang H, Zhang H, Shi L, Liu G, Liu H, Zhao G, Li M and Ye J 2016 Targeted Synthesis of 2H- and 1T-Phase MoS2 Monolayers for Catalytic Hydrogen Evolution *Advanced Materials* **28** 10033–41

[60] Liang Y and Yang L 2015 Carrier Plasmon Induced Nonlinear Band Gap Renormalization in Two-Dimensional Semiconductors *Phys. Rev. Lett.* **114** 063001

[61] Yao K, Yan A, Kahn S, Suslu A, Liang Y, Barnard E S, Tongay S, Zettl A, Borys N J and Schuck P J 2017 Optically Discriminating Carrier-Induced Quasiparticle Band Gap and Exciton Energy Renormalization in Monolayer MoS2 *Phys. Rev. Lett.* **119** 087401

[62] Rao R, Islam A E, Singh S, Berry R, Kawakami R K, Maruyama B and Katoch J 2019 Spectroscopic evaluation of charge-transfer doping and strain in graphene/MoS2 heterostructures *Phys. Rev. B* **99** 195401

[63] Yau S, Lee Y, Chang C, Fan L, Yang Y and Dow W-P 2009 Structures of Aniline and Polyaniline Molecules Adsorbed on Au(111) Electrode: as Probed by in Situ STM, ex Situ XPS, and NEXAFS *J. Phys. Chem. C* **113** 13758–64

[64] Nanayakkara S U, van de Lagemaat J and Luther J M 2015 Scanning Probe Characterization of Heterostructured Colloidal Nanomaterials *Chem. Rev.* **115** 8157–81

[65] Guo C, Pan J, Li H, Lin T, Liu P, Song C, Wang D, Mu G, Lai X, Zhang H, Zhou W, Chen M and Huang F 2017 Observation of superconductivity in 1T′-MoS2 nanosheets *J. Mater. Chem. C* **5** 10855–60

[66] Saigal N, Wielert I, Čapeta D, Vujičić N, Senkovskiy B V, Hell M, Kralj M and Grüneis A 2018 Effect of lithium doping on the optical properties of monolayer MoS2 *Applied Physics Letters* **112** 121902

[67] Wu M, Zhan J, Wu K, Li Z, Wang L, Geng B, Wang L and Pan D 2017 Metallic 1T MoS2 nanosheet arrays vertically grown on activated carbon fiber cloth for enhanced Li-ion storage performance *J. Mater. Chem. A* **5** 14061–9

[68] Jiang L, Zhang S, Kulinich S A, Song X, Zhu J, Wang X and Zeng H 2015 Optimizing Hybridization of 1T and 2H Phases in MoS2 Monolayers to Improve Capacitances of Supercapacitors *Materials Research Letters* **3** 177–83

[69] Li S-L, Komatsu K, Nakaharai S, Lin Y-F, Yamamoto M, Duan X and Tsukagoshi K 2014 Thickness Scaling Effect on Interfacial Barrier and Electrical Contact to Two-Dimensional MoS2 Layers *ACS Nano* **8** 12836–42